16th World Conference on Earthquake, 16WCEE 2017

Santiago Chile, January 9th to 13th 2017

Paper N° 3390

Registration Code: S-B1461839875

A RECONSTRUCTION-FREE SUB-NYQUIST SENSING APPROACH FOR EARTHQUAKE DAMAGE DETECTION USING THE MUSIC ALGORITHM

K. Gkoktsi(1), A. Giaralis(2), B. Tausiesakul(3)

(1) *Dept. of Civil Engineering, City University London, Northampton Square, EC1V 0HB, London, UK, Kyriaki.Gkoktsi.1@city.ac.uk*
(2) *Dept. of Civil Engineering, City University London, Northampton Square, EC1V 0HB, London, UK, Agathoklis.Giaralis.1@city.ac.uk*
(3) *Dept. of Electrical Engineering, Srinakharinwirot University, Ongkharak Campus, Rangsit-Nakhonnayok Road, Ongkharak district, Nakhon Nayok Province, 26120, Bangkok, Thailand, bamrungt@g.swu.ac.th*

Abstract

Motivated by a need to reduce energy consumption in wireless sensors used for Vibration-based Structural Health Monitoring (V-SHM) in seismically prone areas, this paper explores the potential of a recently established sampling scheme, termed co-prime sampling, in conjunction with the multiple signal classification (MUSIC) pseudo-spectrum for earthquake-induced structural damage detection. Firstly, co-prime sampling is adopted to acquire noise-corrupted response acceleration measurements of low-amplitude white-noise excited structures before and after an earthquake, treated as stationary stochastic processes in agreement with the operational modal analysis theory. The obtained measurements are acquired by two different samplers per recording channel operating at different uniform sampling rates, $1/(N_1T)$ and $1/(N_2T)$, where N_1 and N_2 are co-prime numbers and $1/T$ is the Nyquist frequency rate used in conventional sampling schemes. The adopted sampling strategy accumulates samples at an average sub-Nyquist rate (i.e., $1/(N_1T)+1/(N_2T) < 1/T$), supporting the use of arrays of wireless sensors of reduced power consumption associated with data acquisition and wireless transmission rate. Secondly, the MUSIC super-resolution spectral estimator is used to identify up to N_1N_2 structural natural frequencies with resolution $1/(N_1N_2T)$ from the auto-correlation function of the sub-Nyquist measurements without taking any (typically computationally expensive) signal reconstruction step in the time-domain, as required by various recently proposed in the literature sub-Nyquist compressive sensing-based approaches for structural health monitoring, while filtering out any broadband noise added during data acquisition. It is assumed that within the short pre- and post- earthquake time interval, the environmental conditions remain the same and thus any (likely to be slight) change to the natural frequencies detected by the proposed approach can be related to damage due to the input seismic action to the structure.

The applicability of the proposed approach is numerically illustrated using a white-noise excited linear reinforced concrete 3-story frame in a healthy and two damaged states caused by ground motions of increased intensity. The damaged states are represented by linear finite element models with reduced effective flexural rigidities at plastic hinge zones, computed by non-linear response history analysis and the Takeda hysteretic model. The furnished numerical results demonstrate that the considered approach can detect structural damage manifested by changes to the natural frequencies as minor as 1% directly from the sub-Nyquist measurements even for additive white noise of SNR=10dB. These results suggest that the adopted approach makes a dependable noise-immune structural damage detection technique that can be potentially embedded within arrays of wireless sensors for cost-efficient (in terms of data sampling and wireless transmission rates) vibration-based structural health monitoring in seismically prone regions.

Keywords: structural health monitoring; earthquake damage detection; spectral estimation; co-prime sampling; wireless sensors

1. Introduction

Vibration-based structural health monitoring (V-SHM) techniques are commonly used in practice to capture changes to the structural properties of critical civil engineering structures caused by long-term ageing/degradation under operational conditions [1]. In the past three decades, a plethora of damage detection algorithms have been developed and applied in practice within the operational modal analysis (OMA) framework, often referred to as output-only modal analysis or system identification [1-3]. These algorithms aim to detect changes to the structural dynamic properties (e.g. natural frequencies and mode shapes) by processing acceleration response signals of linearly vibrating structures under low-amplitude ambient excitations, commonly modeled as broadband white noise stochastic processes. Importantly, some of the OMA algorithms and techniques proved useful for rapid condition assessment of instrumented structures in the aftermath of major earthquake events [4-6]. In this respect, it has been argued that the widespread installation of V-SHM systems in engineering structures (buildings, bridges, etc.) in seismically prone areas may be a way to improve the resiliency of communities against the seismic hazard [7]. This consideration can be facilitated by reducing the installation and operational cost of such monitoring systems.

In this regard, the use of wireless sensors/accelerometers is rather promising to achieve low up-front cost and rapid implementations of V-SHM compared to arrays of tethered sensors, especially in large-scale and geometrically complex structures [8, 9]. However, wireless sensors require frequent battery replacement (or expensive local energy harvesting solutions), which increase maintenance costs, while they pose restrictions to the amount of data that can be reliably transmitted due to bandwidth limitations, especially in heavily instrumented structures. It has been recently established that both the above disadvantages of wireless sensors for V-SHM may be addressed in a cost-effective manner by considering compressive sensing (CS)-based data acquisition strategies [10-13] to improve power consumption at sensors by reducing the number of measurements acquired (sampled) and transmitted. In particular, CS contemplates that sparse signals (i.e., signals with significant energy clustering in a number of discrete bands in some domain) can be faithfully represented by non-uniform-in-time random samples acquired at an average sampling rate below the Nyquist frequency (sub-Nyquist sampling). In this regime, the minimum average sampling rate is not governed by the maximum frequency contained in the signal to be acquired (as in the case of the conventional uniform-in-time sampling), but, rather, by the level of signal sparsity. Notably, noiseless response acceleration signals from linear vibrating structures tend to be appreciably sparse in the frequency domain, since their Fourier coefficients with non-negligible magnitudes are well-localized (clustered) about their natural frequencies (see e.g., [14]). Nevertheless, typical CS-based sampling approaches require a computationally demanding signal reconstruction step from the compressed (i.e., sub-Nyquist sampled) measurements, while they are sensitive to additive broadband noise [15] as the latter reduces their sparsity level. Both these shortcomings of CS-based sampling have been effectively addressed by the authors [16-19], by considering signal reconstruction-free sub-Nyquist sensing techniques for OMA and damage detection that enjoy noise immunity. Specifically, the adopted sampling approach in [16-19] relies on non-uniform in time deterministic multi-coset sampling implemented in a single sampling device per measurement channel. This sampling strategy is coupled with spectral estimation applied directly to the sub-Nyquist measurements without posing any signal sparsity requirements.

In this context, and inspired by recent work in radar applications, this paper couples the deterministic sub-Nyquist co-prime sampling scheme in [20] with the multiple signal classification (MUSIC) algorithm for spectral estimation [21] to infer earthquake-induced structural damage by monitoring shifts to the resonant frequencies directly from compressed response acceleration measurements without signal reconstruction in time-domain. Note that, as in the case of multi-coset sampling in [16-19], the herein adopted sampling scheme does not rely on any signal sparsity conditions while it treats the acquired signal as a wide-sense stationary stochastic process (random signal), aiming to acquire/sense its auto-correlation function with the aid of the spatial smoothing technique detailed in [22]. From a theoretical viewpoint, this treatment is consistent with the OMA framework, which assumes stochastic input excitation and linear structural response [1], leading to stochastic structural response processes in accordance with the theory of random vibrations. However, co-prime sampling is fundamentally different from the multi-coset sampling adopted in [16-19], as it considers two sensors per acceleration channel operating at different sub-Nyquist rates and accumulating collectively in time a much smaller number of measurements than a single sensor operating at the Nyquist rate. Notably, the MUSIC algorithm has also been considered in the past for earthquake-induced damage detection in building structures [6], using only conventional sensors to acquire structural acceleration signals at Nyquist rate. Furthermore, this pseudo-spectrum technique has found to outperform conventional FFT-based spectral estimators for V-SHM applications [23-25]. This is because MUSIC is a "super resolution" spectral estimator able to capture very small changes in resonant frequencies of linear structural response acceleration (random) signals between healthy and damaged structural states.

The effectiveness and applicability of the herein proposed approach is numerically assessed by considering simulated acceleration response signals corrupted by different levels of additive white noise, originating from a low-amplitude white-noise excited 3-story reinforced concrete frame building before and after being exposed to a particular ground motion, pertaining to a healthy and to a potentially damaged state, respectively. Two different earthquake intensities are considered through scaling of the input ground motion, yielding different levels of structural damage. Special attention is given in modelling the different levels of earthquake-induced damage, based on localized stiffness degradation at the formed plastic hinge zones, as this is captured by the well-known Takeda hysteretic model in conducting non-linear response history analysis.

The remainder of the paper is organized as follows. Section 2 outlines the theory of the adopted co-prime sampling method along with the spatial smoothing technique for auto-correlation function estimation, and reviews the mathematical details of the MUSIC algorithm. Section 3 furnishes and discusses numerical results obtained by processing noise-corrupted response acceleration signals, originating from a 3-story frame building subjected to seismic excitations of increased intensity. Finally, Section 4 summarizes concluding remarks.

2. Theoretical Background

2.1 Co-prime sampling and auto-correlation estimation of stationary stochastic processes

Let $x(t)$ be a complex-valued wide-sense stationary band-limited stochastic process (or random signal), expressed as a superposition of M sinusoidal functions with frequencies f_i, complex amplitudes A_i, and uncorrelated random phases u_i uniformly distributed in the interval $[0, 2\pi]$, where i=1,2,…,M. That is,

$$x(t) = \sum_{i=1}^{M} A_i e^{j2\pi f_i t + u_i}, \tag{1}$$

where $j = \sqrt{-1}$. Co-prime sampling [20, 22] assumes that the signal $x(t)$ is simultaneously acquired by two sampling devices, operating at different (sub-Nyquist) sampling rates, $1/(N_1T)$ and $1/(N_2T)$, where N_1, N_2 are co-prime numbers ($N_1 < N_2$), and $1/T= 2f_{\max}$ is the Nyquist sampling rate with $f_{\max}$ being the highest frequency component in Eq. (1). The signal $x(t)$ is then divided in time blocks of $(2N_1\text{-}1)N_2T$ duration and, within each such block, only $2N_1+N_2\text{-}1$ samples are retained from a total number of $floor\{2(N_1+N_2)\text{-}1\text{-}N_2/N_1\}$ acquired measurements. The thus retained samples of $x(t)$ from the two different samplers are

$$\begin{aligned} x_1[k] &= x(kN_1T) = \sum_{i=1}^{M} A_i e^{j2\pi f_i kN_1T + u_i} + \eta_1[k], \quad k \in \{0,\ldots,N_2-1\} \\ x_2[l] &= x(lN_2T) = \sum_{i=1}^{M} A_i e^{j2\pi f_i lN_2T + u_i} + \eta_2[l], \quad l \in \{1,\ldots,2N_1-1\} \end{aligned}, \tag{2}$$

where $\eta_1[k]$ and $\eta_2[l]$ are zero-mean complex Gaussian white noise sequences, assumed to have the same power, σ_η^2. Notably, the noise sequences $\eta_1[k]$ and $\eta_2[l]$ in Eq. (2) are added at the output of the two sampling devices and assumed to be uncorrelated with the signals and from each other. In this manner, N_2 samples are obtained from the first device, which operates at sampling rate $1/(N_1T)$. Similarly, $2N_1$-1 samples are retrieved from the second device with sampling rate $1/(N_2T)$. This choice is not arbitrary; it can be shown [20] that the cross-difference set of numbers $\mathrm{S} = \{N_2l - N_1k,\ k \in \{0,\ldots,N_2-1\},\ l \in \{1,\ldots,2N_1-1\}\}$ contains all possible integers within the range $[-N_1N_2, N_1N_2]$. Thus, the cross-correlation function of the sequences $x_1[k]$, $x_2[l]$, whose support involves all the time-lags included in the set S, can be continuously estimated in the above range of interest. To this aim, the sequences in Eq. (2) are first stacked in a vector $\mathbf{y}_n \in \mathbb{C}^{(2N_1+N_2-1)}$ as in

$$\mathbf{y}_n = \left[x_1^{\mathrm{T}}\left[2N_2 n + k\right] \quad x_2^{\mathrm{T}}\left[2N_1 n + l\right] \right]^{\mathrm{T}} = \sum_{i=1}^{M} A_i \; \mathbf{e}(f_i)\; e^{j2\pi f_i N_1 N_2 n T + u_i} + \boldsymbol{\eta}_n , \tag{3}$$

where the superscript “T” denotes column vector, $\boldsymbol{\eta}_n \in \mathbb{C}^{(2N_1+N_2-1)}$ is the vector collecting the noise terms, and $\mathbf{e}(f_i) \in \mathbb{C}^{(2N_1+N_2-1)}$ is given by

$$\mathbf{e}(f_i) = \left[1 \quad e^{j2\pi f_i\, N_1 T} \quad \cdots \quad e^{j2\pi f_i (N_2-1) N_1 T} \quad e^{j2\pi f_i\, N_2 T} \quad \cdots \quad e^{j2\pi f_i (2N_1-1) N_2 T} \right]^{\mathrm{T}} . \tag{4}$$

Notably, in Eq. (3), the inclusion of the non-negative integer index $n \in \mathbb{Z}^*$ allows for arbitrarily placing the co-prime sampling block in time (e.g., for n=0 the time block starts at t=0 and corresponds to the block considered in Eq. (2)). Therefore, an arbitrary large number of blocks (and corresponding vectors $\mathbf{y}_n$) can be used for co-prime sampling a theoretically infinitely long random signal $x(t)$. The position of each block in time depends on the adopted values of n. The autocorrelation matrix of $\mathbf{y}_n$ is given as ([22])

$$\mathbf{R}_{\mathbf{yy}} = \mathrm{E}\left\{ \mathbf{y}_n \; \mathbf{y}_n^{\mathrm{H}} \right\} = \sum_{i=1}^{M} A_i^2 \; \mathbf{e}(f_i)\; \mathbf{e}^{\mathrm{H}}(f_i) + \sigma_\eta^2 \mathbf{I} , \tag{5}$$

in which $\mathbf{I} \in \mathbb{R}^{(2N_1+N_2-1)\times(2N_1+N_2-1)}$ is the identity matrix, the superscript “H” denotes Hermitian matrix transposition, and the mathematical expectation operator $\mathrm{E}\{\cdot\}$ averages over n. In other words, the matrix $\mathbf{R}_{\mathbf{yy}}$ in Eq. (5) is computed by averaging over all the time blocks considered in sampling, within a Monte Carlo-based context.

Next, following the spatial smoothing technique in [22], the autocorrelation matrix in Eq. (5) is first stacked in a column vector, $\mathbf{r}_{\mathbf{y}}$=vec($\mathbf{R}_{\mathbf{yy}}$), with $\mathbf{r}_{\mathbf{y}} \in \mathbb{C}^{(2N_1+N_2-1)^2\times 1}$. Then, the elements of $\mathbf{r}_{\mathbf{y}}$ are sorted and truncated within the range [-N_1N_2, N_1N_2], while the repeated terms are eliminated, so that the integer indices of the exponential terms in Eq. (4) are given in increasing order with no repetition. The thus generated reduced autocorrelation vector $\hat{\mathbf{r}}_{\mathbf{y}}$ (i.e. sorted and truncated), is subsequently divided into i= 1,2,…, N_1N_2+1 overlapping subarrays, $\hat{\mathbf{r}}_{\mathbf{y}_i}$, each consisting of (N_1N_2+1) elements, which are averaged as in

$$\mathbf{R}_{ss} = \frac{1}{N_1 N_2 + 1} \sum_{i=1}^{N_1 N_2 + 1} \hat{\mathbf{r}}_{\mathbf{y}_i} \hat{\mathbf{r}}_{\mathbf{y}_i}^{\mathrm{H}} , \tag{6}$$

to generate the spatially smoothed matrix $\mathbf{R}_{ss} \in \mathbb{C}^{(N_1N_2+1)\times(N_1N_2+1)}$. In the following section, this matrix is used as input to a specific super-resolution spectral estimator to detect the M frequencies f_i , (i= 1,2,…,M), of the considered stochastic process $x(t)$.

2.2 Multiple Signal Classification (MUSIC) algorithm for resonant frequencies estimation

The Multiple Signal Classification (MUSIC) algorithm [21] is a super-resolution pseudo-spectrum estimation method, which relies on the eigenvalue decomposition of autocorrelation matrices estimated by field measurements. For the purposes of this study, the MUSIC algorithm is applied to the autocorrelation matrix $\mathbf{R}_{ss}$ in Eq. (6), which is decomposed as in

$$\mathbf{R}_{ss} = \sum_{i=1}^{M} (\lambda_i + \sigma_\eta^2) \mathbf{v}_i \, \mathbf{v}_i^{\mathrm{H}} + \sum_{i=M+1}^{N_1 N_2 + 1} \sigma_\eta^2 \mathbf{v}_i \, \mathbf{v}_i^{\mathrm{H}} , \tag{7}$$

where the eigenvectors $\mathbf{v}_i$ are orthonormal, i.e. $\mathbf{v}_i \mathbf{v}_j^{\mathrm{H}} = 0$ for $i \neq j$. The first term in Eq. (7) represents the signal sub-space with M eigenvalues $(\lambda_i + \sigma_\eta^2)$, i=1,…,M, and M principal eigenvectors spanning the same subspace with the signal vector in Eq. (4). Likewise, the second term corresponds to the noise sub-space with (N_1N_2-M) identical eigenvalues σ_η^2, and (N_1N_2-M) eigenvectors.

The cost function of the unbiased MUSIC estimator is then given as

$$P_{MUSIC}(f) = \frac{1}{\mathbf{e}^{\mathrm{H}}(f)\cdot\left(\sum_{k=M+1}^{N_1N_2+1}\mathbf{v}_k\mathbf{v}_k^{\mathrm{H}}\right)\cdot\mathbf{e}(f)}. \tag{8}$$

The above estimator (pseudo-spectrum) relies on the orthogonality condition between the signal vectors and the noise sub-space, that is,

$$\mathbf{e}^{\mathrm{H}}(f_i)\cdot\left(\sum_{k=M+1}^{N_1N_2+1}\mathbf{v}_k\right) = 0, \quad i = 1,\ldots,M\ , \tag{9}$$

to attain, theoretically, infinite values at the locations on the frequency axis where the natural frequencies of the considered system lie, i.e. at f=f_i. In practical numerical applications, though, involving errors in solving the eigenvalue problem and other estimation errors, Eq. (8) takes finite values observing sharp peaks at each f_i and resulting in a spectrum-like shape. Limitations of the MUSIC algorithm are the *a priori* knowledge on the number of M signal components required, as well as the increased computational demands of the eigenvalue decomposition in Eq. (7). Nonetheless, the significance of utilizing the MUSIC algorithm together with the co-prime sampling strategy and the spatial smoothing technique lies on its capability to capture up to $M \leq N_1N_2$ natural frequencies in noisy signals, at the high frequency resolution of 1/(N_1N_2T), outperforming conventional approaches at Nyquist rate that can only retrieve up to ($2N_1$+N_2-2) frequencies (see also [22]).

3. Numerical Application

3.1 Adopted structure and seismic action

The planar 3-story single-bay reinforced concrete (RC) frame shown in Fig. 1 is herein considered to illustrate the usefulness and applicability of the signal acquisition and processing techniques reviewed in the previous section for earthquake-induced structural damage detection. The geometrical properties of the frame along with the longitudinal and transverse reinforcement of its beams and columns are also shown in Fig.1. The nominal concrete strength is taken equal to 20MPa. The characteristic steel yielding strength is f_{yk}=400MPa for both the longitudinal and transverse reinforcement and the steel hardening ratio is taken as f_{uk}/f_{yk}=1.15. In computing the axial forces carried by the columns, a gravitational uniform distributed load along the beams equal to 35 kN/m is assumed.

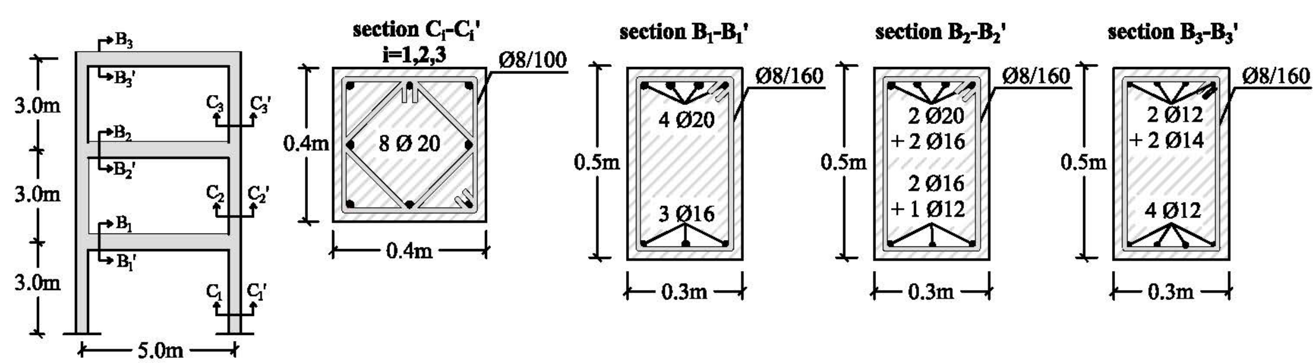

Fig. 1 – Configuration details of the adopted RC frame

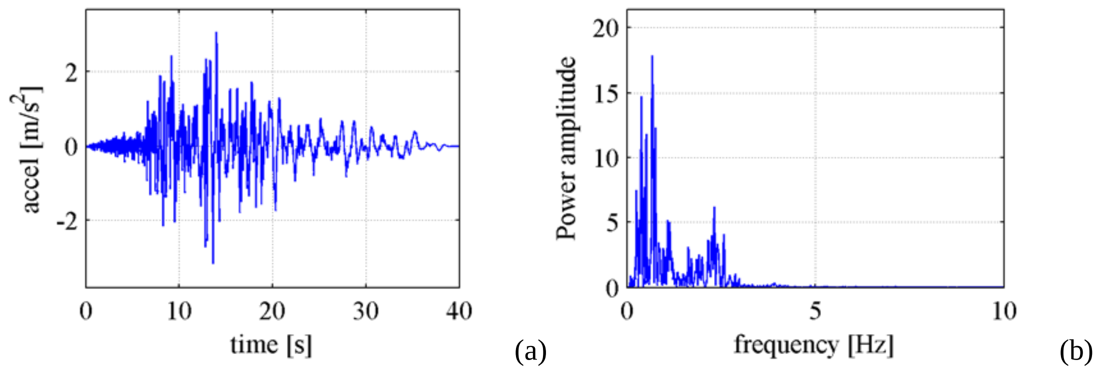

Fig. 2 – Considered Chuetsu-oki (Japan, 2007) horizontal ground motion component: (a) Time-history, (b) Squared amplitude of Fourier spectrum

The structure in Fig.1 is then exposed to the horizontal ground motion (GM) shown in Fig.2 and to a scaled version of this GM by a factor of 0.5, leading to two different levels of structural damage. Notably, the considered (unscaled) GM of Fig.2 was recorded from the "Sanjo Shinbori" station during the M_w=6.8 Chuetsu-oki earthquake (16.7.2007) that occurred in Japan. It has a peak ground acceleration (PGA) equal to 3.17m/s^2 and is characterized by high energy in a wide range of frequencies. The two different damaged states of the structure in Fig.1 are modelled in a finite element (FE) software, as detailed in the following sub-section.

3.2 Finite element modeling of earthquake-induced damage

Non-linear response history analysis (NRHA) is undertaken using the Ruaumoko FE software to quantify the structural damage induced to the structure in Fig.1 due to the earthquake excitation in Fig. 2 scaled by a factor of 0.5 (damaged state 1) and its unscaled version (damaged state 2). To this aim, a non-linear lumped-plasticity FE model is developed, based on the material properties, geometry, and detailing of the considered structure given in the previous sub-section. This is accomplished by first conducting a section analysis to determine the values of the moment capacity- curvature pairs at yielding, M_y-φ_y, and at collapse, M_u-φ_u, at the critical (energy dissipation) zones of all the frame members (i.e., ends of all beams and columns in Fig.1). Then, the secant flexural rigidity at yielding, $EI_y=M_y/\varphi_y$, corresponding to cracked RC sections at all the critical zones are obtained. In this respect, Table 1 reports the average EI_y values of the two ends at each frame member. Next, the plastic hinge length of all critical zones is estimated by the empirical formula [26]

$$L_{pl} = \max\begin{cases} \min\left(0.2(\frac{f_{uk}}{f_{yk}}-1)L_o, 0.08\right) + 0.022 f_{yk} d_{bl} \\ 0.044 f_{yk} d_{bl} \end{cases}, \tag{10}$$

where L_o is the shear span taken herein as half the structural member length, d_{bl} is the diameter of the longitudinal reinforcement, and f_{yk}, f_{uk}/f_{uk} are the steel strength and strain hardening ratio, respectively, given in the previous sub-section. In this study, Eq. (10) yields the value L_{pl}=0.352m for the critical zones in all beams and columns with the exception of the beam at the 3rd story exhibiting plastic zones with L_{pl}=0.246m at both ends.

Table 1 – Average secant flexural rigidity at yielding, EI_y, at the ends of the frame structural members of Fig.1

	Beams			**Columns**		
	1st story	**2nd story**	**3rd story**	**1st story**	**2nd story**	**3rd story**
EI$_y$ **[kNm^2]**	23531	20719	16219	19709	18237	16573

Having obtained the moment capacity-curvature pairs at yielding, M_y-φ_y, and at collapse, M_u-φ_u, as detailed above, non-linear rotational springs with moment-curvature curves, M-φ, governed by the Takeda hysteretic model [27], are used to capture the behavior of the plastic hinges that may develop at the critical zones of the considered frame under seismic excitation. The sections of beams and columns in between the critical zones are modelled as linear-elastic with flexural rigidity equal to EI_y, that is, equal to the secant values at yielding given in Table 1.

NRHA is applied to the developed non-linear FE model for the GM of Fig.2 scaled-down by a factor of 0.5 and for the original GM (unscaled). For both considered GM intensities, it is observed that all beam members yield, while columns remain elastic. In this regard, the inelastic behavior of the considered structure represents well the case of a properly detailed RC frame structure for earthquake resistance. To further illustrate this point and to demonstrate the impact of scaling-down the considered GM by 0.5 in terms of non-linear response behavior, Fig.3 plots the moment-curvature curves at the left plastic hinge on the beam of the 1st story, for the two damaged states considered. Notably, the maximum curvature ductility in Fig. 3(a) is close to unity (i.e., μ_φ=1.45) associated with a very small structural damage near yield. From Fig. 3, it is readily observed that maximum stiffness degradation occurs at the maximum curvature ductility characterized by an effective flexural rigidity, EI_{eff} (slope of red dashed lines in Fig.3), smaller than the secant flexural rigidity at yielding, EI_y (slope of green dashed lines in Fig.3, also reported in Table 1). In this regard, the average ratio EI_{eff}/EI_y (flexural stiffness reduction factor) at the critical zones is herein considered to represent local earthquake-induced damage related to stiffness degradation as captured by the Takeda hysteretic model (which, however, does not take into account the strength deterioration and pinching effects due to cyclic loading). Table 2 presents the thus defined stiffness reduction factors for the two considered damaged states, which yield smaller values within the second case pertaining to a seismic event of increased intensity. As expected, the increased severity of the second damage state reflects on lower values of stiffness reduction factors for the beams, while columns remain practically linear.

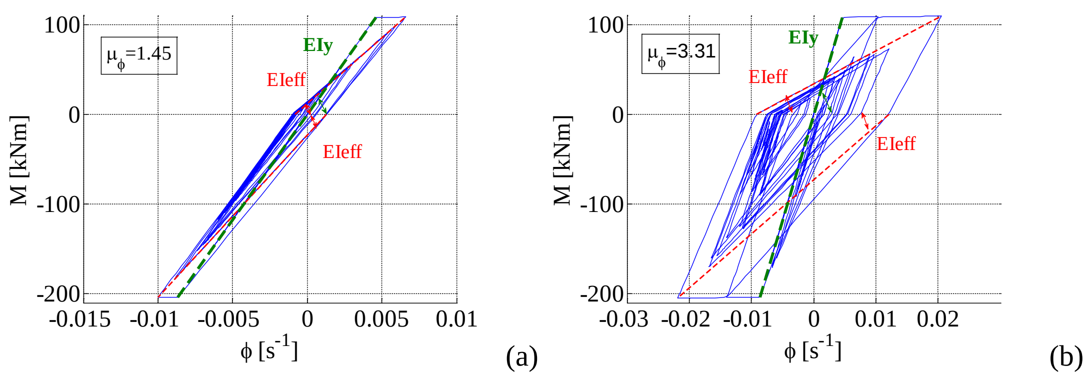

Fig. 3 – Moment-curvature (M-φ) hysteretic curves at the left plastic hinge of the 1st story beam for (a) damage state 1 and (b) damage state 2.

Table 2 – Flexural rigidity reduction factor (EI_{eff}/EI_y) at critical member zones of the structure in Fig.1 for the two different damage states considered due to different seismic intensity excitation

	Beams			**Columns**		
	1st story	**2nd story**	**3rd story**	**1st story**	**2nd story**	**3rd story**
Damaged state 1	0.71	0.53	0.46	1.00	1.00	1.00
Damaged state 2	0.21	0.15	0.17	1.00	1.00	1.00

The reduction factors of Table 2, obtained from NRHA as detailed above, are used to model earthquake-induced structural damage to the structure of Fig.1 due to the two different levels of seismic excitation adopted.

Specifically, two equivalent linear FE models are defined, corresponding to the two different damage states, in which the earthquake-induced damage is represented by means of the flexural stiffness reduction factors of Table 2. In particular, the latter are assigned to linear beam elements of length L_{pl} at the considered plastic hinge zones, while the remaining non-critical frame members exhibit the flexural rigidities in Table 1. Notably, this modelling of local structural damage is deemed more realistic compared to the arbitrary reductions of floor stiffness (i.e., along the whole length of structural members), commonly considered in the relevant literature [25, 28, 29]. Further, it is assumed that the pre-damage/"healthy" state of the considered structure (before the seismic event) is available and is modelled by a linear FE model with the secant flexural rigidities at yield presented in Table 1, which are assigned to the full length of structural members. Moreover, it is assumed that environmental conditions (e.g., temperature, humidity, etc.), whose fluctuations may influence the structural dynamic properties extracted from standard OMA techniques, are the same before and after the seismic event. Thus, in this particular study, any potential change to the modal properties of the considered structure is only associated with the seismic action. The latter assumption is reasonable given the small duration of a typical earthquake and the fact that a power-efficient V-SHM system is installed to the structure supported by sensors sampling at a sub-Nyquist rate, allowing for more frequent data acquisition and processing.

3.3 System identification and damage detection using co-prime sampling and the MUSIC spectrum

Linear response history analyses (LRHA) are undertaken for the three FE models defined in the previous sub-section (healthy plus two damaged states), which are subjected to the same low amplitude white noise base excitation of 80s duration. A time discretization step of 0.01s is taken corresponding to a Nyquist frequency of 50Hz. The considered excitation models ambient wide-band noise input under operational conditions. A critical damping ratio of 5% for all modes of vibration is assumed in the analysis. Horizontal response acceleration signals at all floor levels are recorded with a sampling rate of 100Hz (i.e., 8000 Nyquist measurements per signal) and stored. They are treated as noise-free structural response acceleration time-histories due to ambient noise, field-recorded by sensors located at each floor. Further, these response signals are contaminated with additive Gaussian white noise at three different signal-to-noise ratios (*SNRs*): 10^{20}dB (practically noise-free case), 30dB, and 10dB.

The thus obtained discrete-time noisy response acceleration signals from the healthy and the two damaged states are compressively sensed using the co-prime sampling strategy reviewed in sub-section 2.1. The underlying assumption is that two deployed samplers per recording location are acquiring uniform in time samples of the same signal. Their sampling rates are defined through the co-prime numbers N_1=7 and N_2=11 and are equal to 1/(7T) and 1/(11T), where 1/T= 100Hz is the Nyquist rate. Therefore, the two co-prime samplers accumulate measurements at rate 1/(7T) + 1/(11T) samples per second, which is about 76.6% lower than the Nyquist rate. Further, the assumed co-prime numbers define the cross-difference set $S=\{11\ l-7\ k,\ k\in[0,10],\ l\in[1,13]\}$, which includes all discrete time lags within the support [-77, 77] of the cross-correlation function between the measurements of the two sensors (see also section 2.1). In this study, 492 time blocks are considered in computing the autocorrelation matrix in Eq. (5). Each block contains $(2N_1\text{-}1)\times N_2$=143 Nyquist samples from which only $2N_1+N_2$-1= 24 samples are taken to populate the $\mathbf{R}_{xx}\in\mathbb{R}^{24\times 24}$ matrix. It is noted that a certain level of overlapping between the considered time blocks occurs, given that the structural response acceleration signals are only 8000 Nyquist samples long. However, under the wide-sense stationary assumption and implied ergodicity in the data, this overlapping does not affect the obtained numerical results. Next, the spatially smoothing technique in [22] is employed to generate the semi-positive correlation matrix $\mathbf{R}_{ss}\in\mathbb{R}^{78\times 78}$ in Eq. (6) directly from the coprime-sampled (compressed) measurements. Finally, the MUSIC algorithm reviewed in sub-section 2.2 is applied, by first considering the eigenvalue decomposition of the spatially smoothed matrix $\mathbf{R}_{ss}$ in Eq. (7). Next, the MUSIC estimator in Eq. (8) is evaluated, based on the assumption of M=3 degrees of freedom being present in the acceleration response signals of interest.

Compared to traditional Discrete Fourier Transform (DFT) based spectral estimators, the MUSIC algorithm yields a pseudo-spectrum with sharp peaks corresponding to the natural frequencies of the white-noise excited 3-story frame (following standard OMA and linear random vibrations considerations), while filtering out additive broadband noise. As an example aiming at system identification, Fig. 4 plots the conventional periodograms (DFT-based spectral estimators) of Nyquist sampled response acceleration signals recorded at all floors of the healthy 3-story white-noise excited structure for the extreme additive noise level of *SNR*=10dB, together with MUSIC pseudo-spectra. The latter spectra are obtained from both Nyquist sampled signals (red broken line) and compressively sensed signals (solid blue line) using the approach detailed in section 2. All spectra are normalized to their peak amplitude to facilitate a comparison. It is seen that it is not possible to extract the natural frequencies of the structure from the periodogram of the considered extremely noisy signals sampled at the Nyquist rate. However, the MUSIC pseudo-spectrum estimated directly from the co-prime sampled signals (using less than 76% measurements from the sub-Nyquist rate) can be readily used to detect the resonant natural frequencies of the structure with high resolution, even for this extreme noise level. More importantly, it is found that the MUSIC pseudo-spectrum derived from the Nyquist and the sub-Nyquist sampled signals practically coincide in this case. Thus, the signal information pertaining to the natural frequencies of the system is not lost due to a more than 76% signal compression at acquisition (sub-Nyquist sampling).

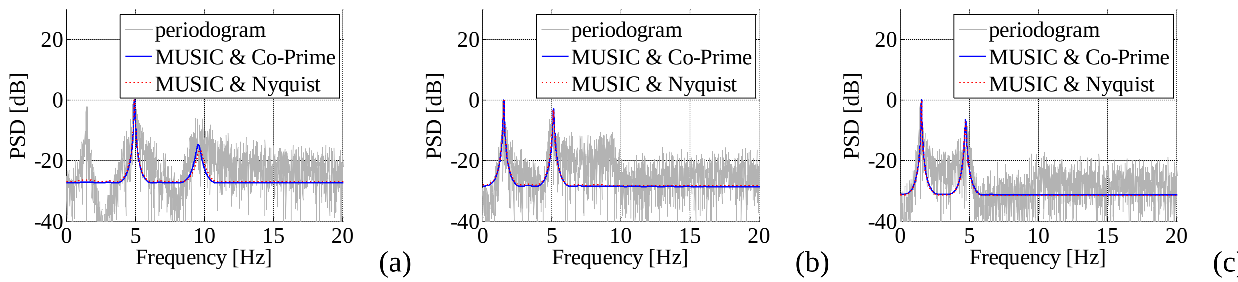

Fig. 4 – Spectrum estimation from noisy acceleration response signals with *SNR*=10dB at (a) the first, (b) second, and (c) third floor of the structure in Fig.1 (healthy state) subject to 80s duration white noise base excitation

Having demonstrated numerically the capability of the MUSIC spectrum to identify structural resonant frequencies from the compressively sensed signals buried in noise, structural damage detection is next pursued based on the shifts of the natural frequencies between the healthy state of the structure in Fig.1, and the two damaged states due to different levels of GM excitation, as detailed in previous sub-sections. For illustration, Figs.5 and 6 plot the MUSIC spectra obtained by co-prime sampled measurements for damaged states 1 and 2, respectively, at all three floors (recording locations). The MUSIC spectra of co-prime sampled measurements from the healthy state are superposed in all panels of Figs. 5 and 6. In all plots, a shift of the natural frequencies towards smaller values (more flexible structure) is evident indicating structural damage. Apparently, these shifts are relatively much smaller for the damage state 1 (i.e., lighter damage due to the scaled-down input GM), rendering the damage detection problem as a more challenging task. It is further important to note that in each panel of Figs.5 and 6 only two out of the expected three structural natural frequencies are detected. Specifically, the MUSIC spectra at the first floor do not capture the first (fundamental) natural frequency, while the spectra at the 2nd and the 3rd floor do not capture the highest (third) natural frequency. In this regard, the three natural frequencies, for each of the three different FE models considered, are estimated by averaging the natural frequency values obtained from the MUSIC spectra across all three floors. Tables 3 and 4 report the thus estimated three natural frequencies (i.e., averaged over the three floors) for the different FE models and for three different *SNR* levels i.e. 10^{20}dB (practically noise-free case), 30dB, and 10dB. The "exact" natural frequencies obtained from standard modal analysis in Ruaumoko are also reported. It is seen that the MUSIC algorithm coupled with co-prime sampling can retrieve the underlying resonant frequencies of the adopted frame in the three considered structural states (i.e., one healthy and two damage states, respectively), with a small error of 1-5% with respect to the exact solution. More importantly, the furnished numerical data show that the proposed methodology is capable to infer earthquake-induced structural damage from small changes to the natural frequencies without being affected by the noise level. This is verified by the fact that the *differences* of the natural frequencies between the healthy and damaged states, as detected by the MUSIC spectra from the co-prime sampled measurements and as computed from the exact values, are almost the same within the wide range of *SNRs* considered (see also the percentage error in Tables 3 and 4).

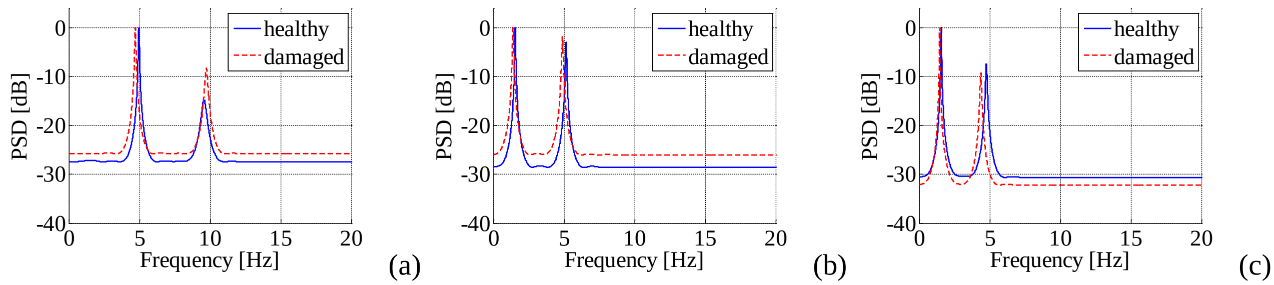

Fig. 5 – MUSIC pseudo-spectra with co-prime sampling of noisy acceleration response signals with *SNR*=10dB at (a) the first, (b) second, and (c) third floor for the healthy and the damaged state 1 structure in Fig.1

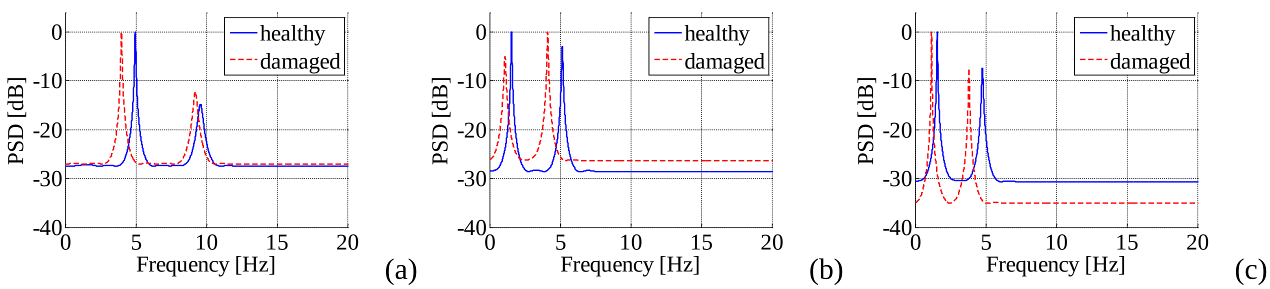

Fig. 6 – MUSIC pseudo-spectra with co-prime sampling of noisy acceleration response signals with *SNR*=10dB at (a) the first, (b) second, and (c) third floor for the healthy and the damaged state 2 structure in Fig.1

Table 3 – Assessment of MUSIC spectra from co-prime sampled noisy measurements for damage detection based on structural natural frequency shifts: damage state 1

***SNR* [dB]**		**f_1 [Hz]**		***error***	**f_2 [Hz]**		***error***	**f_3 [Hz]**		***error***
	state	**healthy**	**Damaged**	**[%]**	**healthy**	**Damaged**	**[%]**	**healthy**	**damaged**	**[%]**
∞	**exact**	1.51	1.40	7%	4.96	4.62	7%	9.68	9.46	2%
10^{20}	**MUSIC**	1.56	1.44	8%	4.97	4.67	6%	9.69	9.76	1%
30		1.56	1.43	8%	4.97	4.67	6%	9.68	9.75	1%
10		1.56	1.43	8%	4.96	4.66	6%	9.58	9.74	2%

Table 4 – Assessment of MUSIC spectra from co-prime sampled noisy measurements for damage detection based on structural natural frequency shifts: damage state 2

***SNR* [dB]**		**f_1 [Hz]**		***error***	**f_2 [Hz]**		***error***	**f_3 [Hz]**		***error***
	state	**healthy**	**damaged**	**[%]**	**healthy**	**damaged**	**[%]**	**healthy**	**damaged**	**[%]**
∞	**exact**	1.51	1.07	29%	4.96	3.97	20%	9.68	9.09	6%
10^{20}	**MUSIC**	1.56	1.13	27%	4.97	3.98	20%	9.69	9.38	3%
30		1.56	1.13	28%	4.97	3.98	20%	9.68	9.36	3%
10		1.56	1.13	28%	4.96	3.97	20%	9.58	9.21	4%

4. Concluding Remarks

A novel earthquake-induced structural damage detection approach was proposed, based on changes to the structural natural frequencies, before and after a seismic event, identified from low amplitude structural response acceleration signals within an operational modal analysis framework. It is assumed that within this short time interval (i.e., pre- and post- earthquake), the environmental conditions remain the same and thus any (likely to be slight) change to the natural frequencies is caused by the input seismic action to the structure. The considered approach employs a compressive/sub-Nyquist sensing technique (co-prime sampling) to acquire response signal measurements, treated as stationary stochastic processes in agreement with the operational modal analysis theory, at a much lower average rate than the Nyquist frequency rate currently used in practice for the task. Further, the adopted approach relies on the MUSIC super-resolution pseudo-spectrum to identify the structural natural frequencies directly from compressive (sub-Nyquist) measurements without taking any (typically computationally expensive) signal reconstruction step in the time-domain, as required by recently proposed in the literature compressive sensing based approaches for structural health monitoring. Moreover, any additive broadband noise during data acquisition does not affect the damage detection capabilities of the proposed approach (at least for the noise levels encountered in practical applications) as such kind of noise is filtered out by application of the MUSIC spectral estimator.

The effectiveness and applicability of the approach was numerically evaluated using a white-noise excited linear reinforced concrete 3-story frame in a healthy and two damaged states caused by two ground motions of increased intensity. The damaged models were simulated with locally reduced effective flexural rigidities (i.e., along the plastic hinge zones), computed by non-linear response history analysis and the Takeda hysteretic model. The furnished numerical results demonstrate that the considered approach is capable to detect very small structural damage directly from the compressed measurements even for high noise levels at *SNR*=10dB. These results suggest that the adopted approach makes a dependable noise-immune structural damage detection technique that can be potentially embedded within arrays of wireless sensors for cost-efficient (in terms of data sampling and wireless transmission rates) V-SHM in seismically prone regions.

5. Acknowledgements

This work has been funded by EPSRC in UK, under the grand No EP/K023047/1. The first author acknowledges the support of City University London through a PhD studentship.

6. References

[1] Brincker R, Ventura CE (2015): *Introduction to Operational Modal Analysis*. Chichester, UK: John Wiley & Sons, Ltd.

[2] Doebling SW, Farrar CR, Prime MB (1988): A summary Review of Vibration-Based Damage ldentification Methods. *Shock Vib. Dig.*, **30** (2), 91–105.

[3] Sohn H, Farrar CR, Hemez F, Czarnecki J (2002): A Review of Structural Health Monitoring Literature 1996 – 2001. *Third World Conf. Struct. Control*, 1–7, Como, Italy.

[4] Rainieri C, Fabbrocino G, Manfredi G, Dolce M (2012): Robust output-only modal identification and monitoring of buildings in the presence of dynamic interactions for rapid post-earthquake emergency management. *Eng. Struct.*, **34**, 436–446.

[5] Foti D, Gattulli V, Potenza F (2014): Output-Only Identification and Model Updating by Dynamic Testing in Unfavorable Conditions of a Seismically Damaged Building. *Comput. Civ. Infrastruct. Eng.*, **29** (9), 659–675.

[6] Jiang X, Adeli H (2007): Pseudospectra, MUSIC, and dynamic wavelet neural network for damage detection of highrise buildings. *Int. J. Numer. Methods Eng.*, **71** (5), 606–629.

[7] Gattulli V, Potenza F, Graziosi F, Federici F, Colarieti A, Faccio M (2014): Distributed Structural Monitoring for a Smart City in a Seismic Area. *Key Eng. Mater.*, **628**, 123–135.

[8] Lynch JP (2007): An overview of wireless structural health monitoring for civil structures. *Philos. Trans. R. Soc. A Math. Phys. Eng. Sci.*, **365** (1851), 345–372.

[9] Spencer BF, Yun C (2010): Wireless Sensor Advances and Applications for Civil Infrastructure Monitoring. *Newmark Structural Engineering Laboratory*, University of Illinois, Urbana-Champaign.

[10] O'Connor SM, Lynch J.P, Gilbert AC (2014): Compressed sensing embedded in an operational wireless sensor network to achieve energy efficiency in long-term monitoring applications. *Smart Mater. Struct.*, **23** (8), 085014.

[11] Park JY, Wakin MB, Gilbert A.C (2014): Modal analysis with compressive measurements. *IEEE Trans. Signal Process.*, **62** (7), 1655–1670.

[12] Yang Y, Nagarajaiah S (2015): Output-only modal identification by compressed sensing: Non-uniform low-rate random sampling. *Mech. Syst. Signal Process.*, **56–57**, 15–34.

[13] Zou Z, Bao Y., Li H, Spencer BF, Ou J (2015): Embedding compressive sensing-based data loss recovery algorithm into wireless smart sensors for structural health monitoring. *IEEE Sens. J.*, **15** (2), 797–808.

[14] Gkoktsi K, Giaralis A (2016): Effect of frequency domain attributes of wavelet analysis filter banks for structural damage localisation using the relative wavelet entropy index. *Int. J. Sustainable Mat. Struct. Sys.* (accepted).

[15] Davenport MA, Laska JN, Treichler JR, Baraniuk RG (2012): The Pros and Cons of Compressive Sensing for Wideband Signal Acquisition: Noise Folding versus Dynamic Range. *IEEE Trans. Signal Process.*, **60** (9), 4628–4642.

[16] Tausiesakul B, Gkoktsi K, Giaralis A (2014): Compressive Sensing Spectral Estimation For Output-Only Structural System Identidication. *7th International Conference on Computational Stochastic Mechanics*, 1–12, Santorini, Greece.

[17] TauSiesakul B, Gkoktsi K., Giaralis A (2015): Compressive power spectrum sensing for vibration-based output-only system identification of structural systems in the presence of noise. *SPIE Sensing Technology + Applications*, Baltimore, US.

[18] Gkoktsi K, TauSiesakul B, Giaralis A (2015): Multi-channel sub-Nyquist cross-Spectral Estimation for Modal Analysis of Vibrating Structures. *International Conference on Systems, Signals and Image Processing (IWSSIP 2015)*, London, UK.

[19] Gkoktsi K, Giaralis A, TauSiesakul B (2016): Sub-Nyquist signal-reconstruction-free operational modal analysis and damage detection in the presence of noise. *SPIE Smart Structures and Materials + Nondestructive Evaluation and Health Monitoring*, 980312, Las Vegas, US.

[20] Vaidyanathan PP, Pal P (2011): Sparse Sensing With Co-Prime Samplers and Arrays. *IEEE Trans. Signal Process.*, **59** (2), 573–586.

[21] Marple SL (1987): *Digital spectral analysis*. Englewood Cliffs, London: Prentice-Hall.

[22] Pal P, Vaidyanathan PP (2011): Coprime sampling and the music algorithm. *2011 Digit. Signal Process. Signal Process. Educ. Meet. DSP/SPE 2011 - Proc.*, **0** (1), 289–294.

[23] Camarena-Martinez D, Amezquita-sanchez JP, Valtierra-rodriguez M, Romero-troncoso RJ, Osornio-rios RA, Garcia-perez A (2014): EEMD-MUSIC-Based Analysis for Natural Frequencies Excitations. *Sci. World J.*, **2014**, 1–12.

[24] Amezquita-Sanchez JP, Garcia-Perez A, Romero-Troncoso RJ, Osornio-Rios RA, Herrera-Ruiz G (2012): High-resolution spectral-analysis for identifying the natural modes of a truss-type structure by means of vibrations. *J. Vib. Control*, **19** (16), 2347–2356.

[25] Humar J (2006): Performance of Vibration-based Techniques for the Identification of Structural Damage. *Struct. Heal. Monit.*, **5** (3), 215–24.

[26] Priestley MJN, Calvi GM, Kowalsky MJ (2007): *Displacement-based seismic design of structures*. IUSS Press.

[27] Takeda, Sozen, Nielsen (1970): Reinforced Concrete Response to Simulated Earthquakes. *Journal of the Structural Division*, **96** (12), 2557–2573.

[28] Loh CH, Chan CK, Lee CH (2016): Application of time series based damage detection and localization algorithms to structures under ambient excitations. *SPIE Smart Structures and Materials + Nondestructive Evaluation and Health Monitoring*, 98031Q, Las Vegas, US.

[29] Yan G, Duan Z, Ou J, De Stefano A (2010): Structural damage detection using residual forces based on wavelet transform. *Mech. Syst. Signal Process.*, **24** (1), 224–239.